

Contents

Contents	i
1 Introduction	1
1.1 A brief history of superfluidity	1
1.2 Some key concepts	3
1.2.1 Bose-Einstein condensation and long-range order	4
1.2.2 Bogolyubov's approximation and the order parameter	5
1.2.3 Landau's criterion for superfluidity	6
1.2.4 Rotation and vorticity in superfluids	8
1.3 Helium droplets	10
Part I Photo-excitation dynamics of alkalis	13
2 Alkali-doped nanodroplets	15
2.1 Experimental setup	15
Part II Capture by quantised vortices	19
3 Quantised vortices in droplets	21
Bibliography	23

Chapter 1

Introduction

SUPERFLUIDS are liquids and gases with remarkable properties. In particular, superfluid helium can flow through a capillary without friction due to its extremely small viscosity (at least 1500 times smaller than normal liquid helium^[1]), or creep up the wall of a container, seemingly defying the force of gravity^[2] (“Rollin creeping”). Its thermal conductivity is about 3×10^6 times higher than that of liquid helium I or about 200 times higher than that of copper at room temperature^[3]. It therefore earned the title of “best heat conducting substance we know” by Willem and his daughter Anna Keesom and dubbed “*supra-heat-conducting*”^[3]. Later it was understood why^[4-7] and it turns out that heat doesn’t diffuse through the medium as in normal liquids, but rather it travels through the medium in waves (second sound). This makes it an ideal coolant e.g. to stabilise the superconducting magnets in CERN’s Large Hadron Collider^[8]. Helium is also the only known substance that stays liquid at zero temperature and low pressures and both its angular momentum and vorticity are quantised, making it the first observed macroscopic quantum substance. Helium-4 becomes superfluid below the λ -point, named so by William H. Keesom in 1936 who measured a singularity in the specific heat at $T_\lambda = 2.2\text{ K}$ ^[3].

1.1 A brief history of superfluidity

HELIUM was the last gas to be liquefied and was done so by Heike Kamerlingh Onnes in 1908^[11,12]. In 1932 John McLennan saw that liquid helium stopped boiling below $\approx 2.2\text{ K}$ ^[13] and later that year Willem Keesom and his daughter Anna observed, while measuring the temperature dependence of the specific heat, a singularity around the same temperature^[9]. They called it the “ λ -temperature”, T_λ , because of the shape of the temperature dependence of the specific heat resembling the Greek letter λ (see Figure 1.1). A few years later in 1935 Burton measured a sharp decrease in the viscosity of liquid helium below T_λ ^[14]. Around the same time Fritz London was already thinking about macroscopic wave functions and why helium does not freeze at $T = 0\text{ K}$ under atmospheric pressure^[15]. London and Simon concluded that it was caused by the zero point motion of the helium atoms and their associated kinetic energy that is comparable to their Van der Waals energy, effectively preventing liquid helium to solidify^[16,17]. The year after, in 1936, Willem and Anna Keesom measured an abnormally high heat conductance below T_λ ^[3]. This was confirmed roughly one year later by J.F. Allen *et al.*^[18] and it was understood that the high thermal conductance was the reason for the helium to stop boiling whenever the temperature drops below T_λ . It was in 1937, when Kapitza tried to determine the viscosity of the laminar flow, that he measured a viscosity that was about 10^4 times smaller than that of hydrogen gas^[1]. It was then that Kaptiza who, by

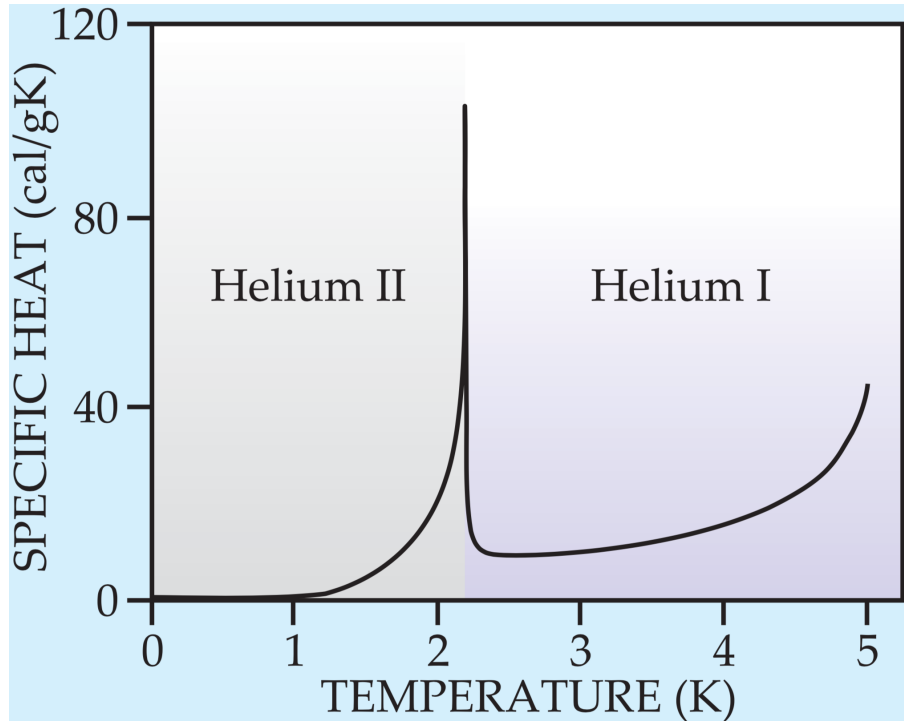


Figure 1.1: The specific heat of ${}^4\text{He}$ as a function of the temperature. There is a clearly visible singularity around 2.2 K and the graph itself has the distinct λ -like shape that inspired^[9] Willem and Anna Keesom to call the temperature at which the singularity occurs the “ λ -point”. (Illustration courtesy of R.J. Donnelly^[10])

analogy with superconductors, first coined the word “superfluid”^[1] to describe the special state that helium enters below the λ -point where it can flow, seemingly without friction. Allen and Misener realised that superfluid helium is not just a liquid with a very low viscosity, but that its hydrodynamics was completely different from that of ordinary liquids^[19] and therefore required a completely new interpretation.

The start of this new interpretation was made by London^[20] in 1938 when he made a connection between the behaviour of superfluid helium and that of an ideal “Bose-Einstein” (BE) gas. Both his calculated value for $T_c = 3.09$ K and the behaviour of the temperature dependence of the heat capacity for the ideal BE-gas were very similar to the measured ones for liquid helium below T_λ . He wrote to Nature that “it was difficult not to imagine a connection with “Bose-Einstein condensation” (BEC). Tisza expanded upon London’s ideas^[21] and considered a Helium II system of total N atoms to consist of two parts; a macroscopic “condensed” part n_0 , the superfluid component, in the ground state, and the remaining part $n = N - n_0$, the normal component, where the helium atoms are distributed over the excited states. Assuming this was correct the fraction n_0/N should decrease with increasing temperature according to the equation

$$\frac{n_0}{N} = 1 - \left(\frac{T}{T_0} \right)^s \quad \text{for } T < T_0 \quad (1.1)$$

where $s = 3/2$ for an ideal gas and should be taken larger, e.g. $s = 5$, for a real liquid with stronger interactions between the atoms.

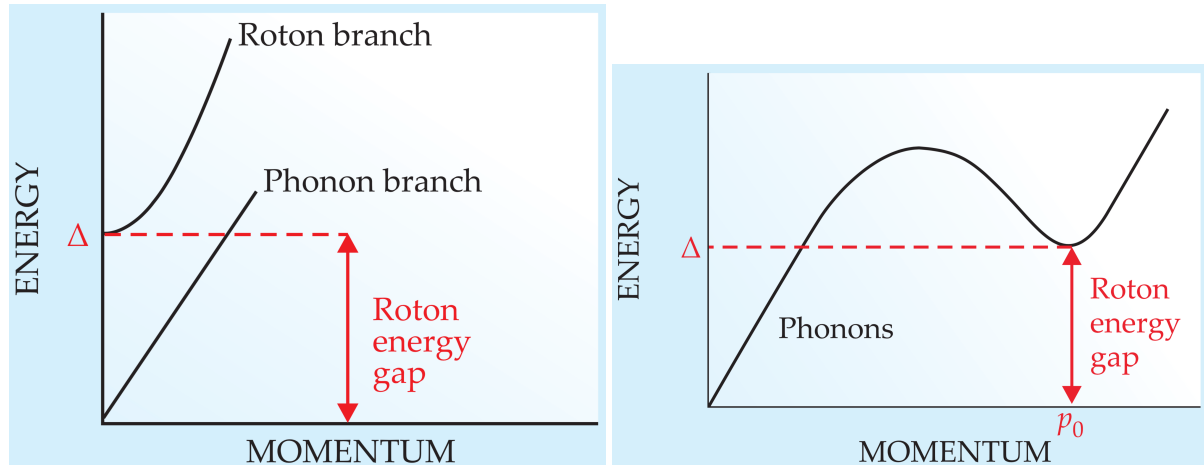


Figure 1.2: Left: Lev Landau’s 1941 energy dispersion curve [22] for the excitations in liquid helium below T_λ . It exhibits a phonon- and a roton branch. The slope of the linear phonon branch corresponds to the velocity of sound. Right: Lev Landau’s 1947 modified dispersion curve. The roton-branch is no longer a separate excitation branch but rather an extension of the phonon-branch. (Illustration courtesy of R.J. Donnelly^[10])

This was the birth of the “two-fluid” model. With this model he derived two hydrodynamic equations for liquid helium below T_λ and discovered that within it, heat propagates in waves instead of diffusing through the medium, and calculated the velocity of these waves. He also explained why the viscosity is disappearing at low temperatures contrary to classical liquids where the viscosity increases^[4–7]. In 1941 Lev Landau reformulated Tisza’s theory on a more rigorous footing^[22,23]. He assumed, contrary to Tisza, that the normal component of the liquid was made-up of collective excitations instead of excited single atoms. He postulated that the liquid could exhibit two states of motion which he called “potential motion” that is irrotational ($\nabla \times \mathbf{v} = 0$), and “vortex motion” that is rotational ($\nabla \times \mathbf{v} \neq 0$). The corresponding energies of these two motions are discontinuously separated by an energy gap Δ . In case of potential internal motion the excitations are quanta of longitudinal (sound) waves, i.e., phonons. The excitations of the vortex-spectrum could be called “rotons” (see Figure 1.2).

A theoretical demonstration, explicitly showing that phonons and rotons are collective excitations of the liquid, came in the form of a 1947 paper by Nikolay Bogolyubov^[24]. The intimate relationship between superfluidity and BEC was not universally accepted until 1995 when Cornell and Wieman in Colorado and Ketterle at MIT discovered BEC in rubidium quantum gases^[25,26].

1.2 Some key concepts

In this section I will briefly introduce some key ideas that are used throughout the thesis and that are needed to fully appreciate the discussed material. Also references to more complete and more in-depth treatments will be provided for the interested reader.

1.2.1 Bose-Einstein condensation and long-range order

The essential concept of Bose-Einstein (BE) condensation is the fact that at low temperatures, multiple bosons, unlike fermions, will occupy the same quantum state. In theory there is no upper bound of how many bosons can occupy such a single state. It is then said that, with ever decreasing temperature, a macroscopic part of the total number of bosons will “condense” into the quantum state with the lowest energy.

Another important concept in BEC is the idea of long-range order. Let us start by introducing the one-body density matrix of a system of N bosons in a pure state $\Psi_k(\mathbf{r}_1, \mathbf{r}_2, \dots, \mathbf{r}_N)$

$$n_k^{(1)}(\mathbf{r}, \mathbf{r}') := N \int \Psi_k^*(\mathbf{r}, \mathbf{r}_2, \dots, \mathbf{r}_N) \Psi_k(\mathbf{r}', \mathbf{r}_2, \dots, \mathbf{r}_N) d\mathbf{r}_2 d\mathbf{r}_3 \dots d\mathbf{r}_N \quad (1.2)$$

where the integral is taken over the $N - 1$ coordinates $\mathbf{r}_2, \mathbf{r}_3, \dots, \mathbf{r}_N$. For a statistical mixture of quantum states one needs to take the weighted average over all the different Ψ_k -states. In thermodynamic equilibrium the states are Boltzmann weighted by their eigenvalues $\{E_k\}$

$$n^{(1)}(\mathbf{r}, \mathbf{r}') = \frac{1}{Q} \sum_k n_k^{(1)}(\mathbf{r}, \mathbf{r}') e^{-E_k/k_B T} \quad (1.3)$$

where Q is the partition function. For more general cases the one-body density matrix is defined

$$n^{(1)}(\mathbf{r}, \mathbf{r}') := \langle \hat{\Psi}^\dagger(\mathbf{r}) \hat{\Psi}(\mathbf{r}') \rangle \quad (1.4)$$

where $\hat{\Psi}^\dagger(\mathbf{r})/\hat{\Psi}(\mathbf{r})$ are field-operators creating/annihilating a boson at \mathbf{r} and the averaging $\langle \dots \rangle$ is taken over all states in the mixture. Once it is accepted that a macroscopic part of the total number of bosons can occupy a single quantum state it can be demonstrated that, while considering a uniform isotropic system of N bosons, the one-body density matrix (Eq. 1.2) tends to a constant value when the distance between \mathbf{r} and \mathbf{r}' goes to infinity. In the thermodynamic limit where $N, V \rightarrow \infty$ such that $n = N/V$ is kept fixed, the one-body density only depends on the modulus of the relative variable $\mathbf{s} := \mathbf{r} - \mathbf{r}'$ so that we can write it as the Fourier transform of the momentum distribution as

$$n^{(1)}(s) = \frac{1}{V} \int n^{(1)}(\mathbf{p}) \exp(i\mathbf{p} \cdot \mathbf{s}/\hbar) d\mathbf{p} \quad (1.5)$$

For a BEC system, the momentum distribution at small momenta is not smooth but has a sharp peak around $p = 0$ for the bosons that are in the ground state, while the remaining bosons are smoothly distributed over the excited states.

$$n(\mathbf{p}) = N_0 \delta(\mathbf{p}) + \tilde{n}(\mathbf{p}) \quad (1.6)$$

where \tilde{n} is a smoothly varying function of \mathbf{p} . When this expression is plugged into Eq. (1.5) and taking the limit where s goes to infinity

$$\lim_{s \rightarrow \infty} n^{(1)}(s) = \frac{N_0}{V}, \quad (1.7)$$

where $N_0/V := n_0 \leq 1$ is called the condensate fraction. It is called long-range order since it involves the off-diagonal elements of the one-body density matrix; the elements that are usually associated with the coherences.

A set of eigenvalues $\{n_i\}$ of the one-body density matrix can be defined through the following eigenvalue equation

$$\int n^{(1)}(\mathbf{r}, \mathbf{r}') \varphi_i(\mathbf{r}') d\mathbf{r}' = n_i \varphi_i(\mathbf{r}) \quad (1.8)$$

and its solutions $\{\varphi_i\}$ form a natural orthonormal basis set of single boson wave functions $\int \varphi_i^* \varphi_j d\mathbf{r} = \delta_{ij}$, with normalisation condition $\sum_i n_i = N$. This permits writing the one-body density matrix in a useful diagonalised form and recalling that BEC occurs when a single particle state φ_i is occupied in a macroscopic way, say when $n_{i=0} = N_0$, a number of order N , we separate the condensate part from the rest

$$n^{(1)}(\mathbf{r}, \mathbf{r}') = N_0 \varphi_0^*(\mathbf{r}) \varphi_0(\mathbf{r}') + \sum_{i \neq 0} n_i \varphi_i^*(\mathbf{r}) \varphi_i(\mathbf{r}') \quad (1.9)$$

1.2.2 Bogolyubov's approximation and the order parameter

It is customary, given the importance of the condensate fraction N_0 in a BEC, to write the field operator of a N -body boson system as the sum of the condensate part and the rest, just as the one-body density matrix

$$\hat{\Psi}(\mathbf{r}) = \varphi_0(\mathbf{r}) \hat{a}_0 + \sum_{i \neq 0} \varphi_i(\mathbf{r}) \hat{a}_i \quad (1.10)$$

where the \hat{a}_i and \hat{a}_i^\dagger are annihilation and creation operator of a particle in state φ_i and obey the usual bosonic commutation relations

$$[\hat{a}_i, \hat{a}_j^\dagger] = \delta_{ij}, \quad [\hat{a}_i, \hat{a}_j] = 0 = [\hat{a}_i^\dagger, \hat{a}_j^\dagger] \quad (1.11)$$

Using Eq. (1.10) in Eq. (1.2) and comparing it to Eq. (1.9) one finds the expectation value of $\langle \hat{a}_j^\dagger \hat{a}_i \rangle = \delta_{ij} n_i$. Now, the Bogolyubov approximation essentially replaces the operators \hat{a}_0 and \hat{a}_0^\dagger with the *c*-number¹ $\sqrt{N_0}$. This is equivalent to ignoring the non-commutative nature of the operators due to the macroscopic occupation of the state φ_0 , when $N_0 = \langle \hat{a}_0^\dagger \hat{a}_0 \rangle \gg 1$. We then rewrite the field operator as the sum of a classical field for the condensed component and quantum field for the non-condensed component

$$\hat{\Psi}(\mathbf{r}) = \Psi_0(\mathbf{r}) + \delta\hat{\Psi}(\mathbf{r}), \quad (1.12)$$

where $\delta\hat{\Psi}(\mathbf{r}) = \sum_{i \neq 0} \varphi_i(\mathbf{r}) \hat{a}_i$ and $\Psi_0(\mathbf{r}) = \sqrt{N_0} \varphi_0(\mathbf{r})$. At $T = 0$ the whole system is condensed and one can ignore $\delta\hat{\Psi}$ altogether; the field operator becomes a normal function of space Ψ_0 .

The classical field Ψ_0 is called the *effective-* or *macroscopic* wave function of the condensate and it behaves like an order parameter in the sense that it varies continuously between a maximum value \sqrt{N} , that is proportional to the total number particles in the system, at $T = 0$, and vanishes at the superfluid-normal fluid phase transition temperature T_λ . It is a complex quantity characterised by a real-valued modulus and phase S :

$$\Psi_0(\mathbf{r}) = \left| \sqrt{N_0} \varphi_0(\mathbf{r}) \right| e^{iS(\mathbf{r})} \quad (1.13)$$

¹The term *c*-number is old nomenclature for a classical number, which can be real or complex, to distinguish them from quantum numbers, or *q*-numbers, that are represented by operators.

The modulus determines the number-density of the condensate, while the phase S plays an important role in the coherence and properties of the superfluid. As we will see in Section 1.2.4, S plays the role of a velocity potential.

Using an order parameter as defined here is equivalent to using the many-body wave function

$$\Phi(\mathbf{r}_1, \mathbf{r}_2, \dots, \mathbf{r}_N) = \prod_{i=1}^N \varphi_0(\mathbf{r}_i), \quad (1.14)$$

with a density operator $\hat{\rho}(\mathbf{r}) := \sum_{i=1}^N \delta(\mathbf{r} - \mathbf{r}_i)$ (see Section ??). One way to see why this wave function plays the role of an order parameter is to look at its time dependence. For normal wave functions the time dependence is determined by the eigenvalues E_i of the Hamiltonian of the system

$$\Psi(\mathbf{r}, t) = \psi(\mathbf{r}) e^{-iE_i t/\hbar} \quad (1.15)$$

But in this case, the time dependence is determined by the chemical potential $\mu = E(N) - E(N-1) \approx \partial E / \partial N$

$$\Psi_0(\mathbf{r}, t) = \Psi_0(\mathbf{r}) e^{-i\mu t/\hbar} \quad (1.16)$$

Another aspect of Ψ_0 being an order parameter and not a true many-body wave function is that two solutions Ψ_a and Ψ_b of the non-linear droplet Hamiltonian corresponding to two different values of the chemical potential μ_a and μ_b are not necessarily orthogonal, i.e. $0 \leq N^{-1} \int \Psi_a^* \Psi_b d\mathbf{r} < 1$. However, in dilute gases it is possible to construct a many-body wave function from the order parameter that regains its orthonormality in the thermodynamic limit

$$\Phi_0(\mathbf{r}_1, \mathbf{r}_2, \dots, \mathbf{r}_N) = \left(\frac{1}{\sqrt{N}} \Psi_0(\mathbf{r}_1) \right) \left(\frac{1}{\sqrt{N}} \Psi_0(\mathbf{r}_2) \right) \dots \left(\frac{1}{\sqrt{N}} \Psi_0(\mathbf{r}_N) \right) \quad (1.17)$$

1.2.3 Landau's criterion for superfluidity

For a gas or liquid to be able to become superfluid Landau postulated that the energy dispersion relation needs to fulfil certain requirements. Specifically for a fluid to flow without dissipation, i.e. a super-flow, the velocity field needs to fulfil the following inequality:

$$v < v_c = \min_{\mathbf{p}} \frac{\epsilon(\mathbf{p})}{p} \quad (1.18)$$

For an ideal Bose gas $\epsilon(\mathbf{p}) = \frac{p^2}{2m}$. In this case

$$v_c = \min_{\mathbf{p}} \frac{\epsilon(\mathbf{p})}{p} \quad (1.19)$$

$$= \min_{\mathbf{p}} \frac{p}{2m} \quad (1.20)$$

$$= 0 \quad (1.21)$$

Apparently ideal Bose-gases cannot become superfluid.

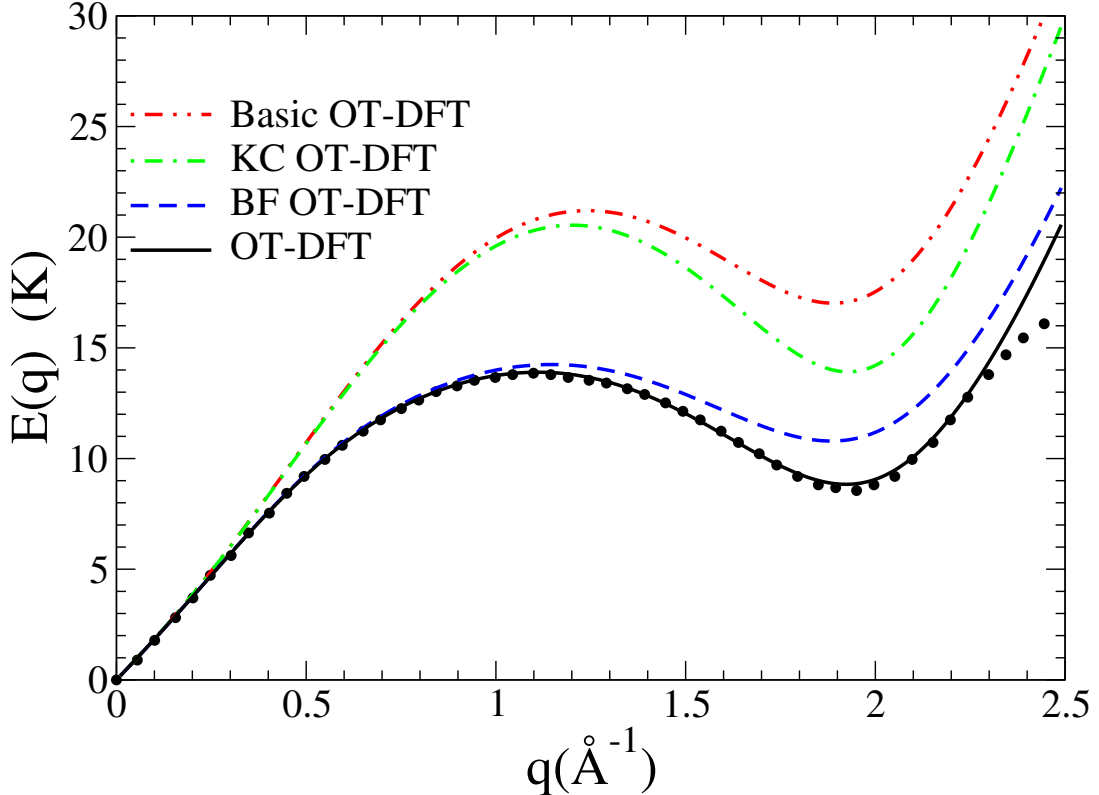


Figure 1.3: Dispersion relation for elementary excitations in liquid ${}^4\text{He}$ calculated as in [27]. ‘Basic’ indicates the OT-DFT without the non-local kinetic energy correlation (KC) nor the back-flow (BF) terms; KC OT-DFT adds to the basic OT-DFT the KC term; BF OT-DFT adds to the basic OT-DFT the BF term. The dots are the experimental data from [28]. The Landau velocity $v_L = E(q)/(\hbar q)|_{min}$ obtained for each functional is 60.3 m/s (OT-DFT); 75.1 m/s (BF OT-DFT); 94.4 m/s (KC OT-DFT); 118 m/s (basic OT-DFT); and 57.5 (experiment).

But if we allow for some weak interactions between the bosons the energy dispersion relation is given by

$$\epsilon(\mathbf{p}) = \sqrt{\frac{gn}{m}p^2 + \left(\frac{p^2}{2m}\right)^2}, \quad (1.22)$$

Bogolyubov’s dispersion law for elementary excitations (1947). And thus

$$v_c = \min_{\mathbf{p}} \sqrt{\frac{gn}{m} + \frac{p^2}{4m^2}} \quad (1.23)$$

$$= \sqrt{\frac{gn}{m}} \quad (1.24)$$

$$= c, \quad (1.25)$$

the speed of sound. Here $g = \frac{4\pi\hbar^2 a}{m}$, and a the s -wave scattering length. The weakly interacting Bose gases can become superfluid.

Liquid helium below the λ -point has a similar energy dispersion relation (see Figure 1.3) hence reinforcing the notion that superfluidity and Bose–Einstein condensation are two intimately related concepts. The experimental value of the speed of sound is ~ 57.5 m/s.

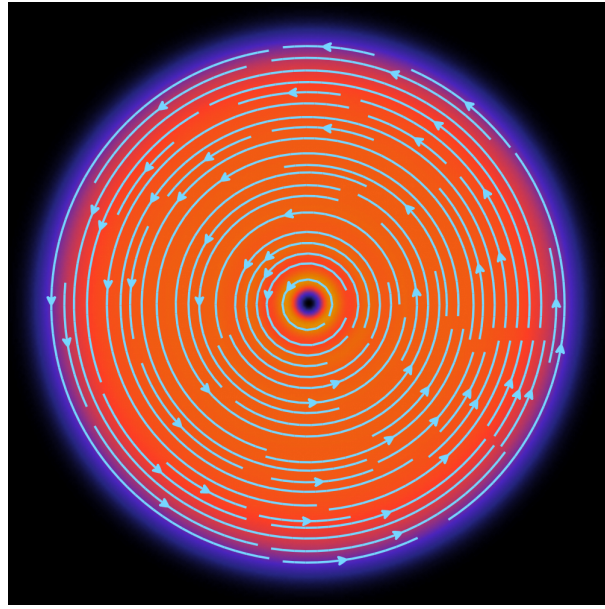


Figure 1.4: Cross section of a ${}^4\text{He}$ droplet through a symmetry plane. The droplet is made of 1000 atoms. Superimposed in cyan are the streamlines of the velocity field \mathbf{v}_s for $s = 1$. They are concentric circles, centred around the vortex core along the z -axis. The colour scale encodes for the density $\rho(r)$. The radius of the droplet is about 22 Å.

1.2.4 Rotation and vorticity in superfluids

Starting from time-dependent Euler-Lagrange (EL) equation (Eq. ??, see Chapter ??) for the time-evolution of the order parameter Ψ (Eq. 1.13, dropping the ground-state subscript and allowing φ and S to vary in time)

$$i\hbar \frac{\partial}{\partial t} \Psi(\mathbf{r}, t) = \left[-\frac{\hbar^2}{2m} \nabla^2 + \frac{\delta \mathcal{E}_c}{\delta \rho} \right] \Psi(\mathbf{r}, t) \quad (1.26)$$

one left-multiplies it with the complex conjugate of the order parameter Ψ^* and then subtract the complex conjugate of the whole expression on both sides. After some algebra and defining $\rho(\mathbf{r}, t) := N|\varphi(\mathbf{r}, t)|^2$, one arrives at the continuity equation

$$\frac{\partial \rho}{\partial t} + \nabla \cdot \mathbf{j} = 0, \quad (1.27)$$

with

$$\mathbf{j}(\mathbf{r}, t) := -\frac{i\hbar}{2m} [\Psi^*(\mathbf{r}, t) \nabla \Psi(\mathbf{r}, t) - \Psi(\mathbf{r}, t) \nabla \Psi^*(\mathbf{r}, t)] \quad (1.28)$$

$$= \rho(\mathbf{r}, t) \frac{\hbar}{m} \nabla S(\mathbf{r}, t) \quad (1.29)$$

From Eq. (1.27) it follows that the atomic number density is a conserved quantity.

We can identify the collective velocity \mathbf{v}_s of the superfluid through the relation

$$\mathbf{v}_s(\mathbf{r}, t) = \mathbf{j}/\rho = \frac{\hbar}{m} \nabla S(\mathbf{r}, t) \quad (1.30)$$

and we see that the rotation of the velocity field of the superfluid $\nabla \times \mathbf{v}_s = 0$, i.e. the fluid is said to be *irrotational*; a typical property of superfluids. Conversely, taking the curl $\nabla \times \mathbf{j} = \frac{\hbar}{m} \nabla \rho \times \nabla S$

we see that this is merely a restatement of the fact that one needs a gas or liquid with a non-uniform density and a non-zero phase for it to be able to support vortices.

Let us consider the illustrative example of a line vortex through the origin along the z -axis. As will be demonstrated in Section ??, this is a stationary state of the droplet Hamiltonian and therefore its time dependence is just a multiplicative factor. In cylindrical coordinates (r, φ, z) such a vortex solution has the form

$$\Psi_s(\mathbf{r}) = \sqrt{\rho(r)} e^{is\varphi}, \quad (1.31)$$

with s an integer. This is an eigenfunction of the angular momentum operator \hat{L}_z with eigenvalue

$$\hat{L}_z \Psi_s(\mathbf{r}) = \frac{\hbar}{i} \frac{\partial}{\partial \varphi} \Psi_s(\mathbf{r}) = \hbar s \Psi_s(\mathbf{r}) \quad (1.32)$$

and with expectation value

$$\langle \hat{L}_z \rangle = \langle \Psi_s | \hat{L}_z | \Psi_s \rangle \quad (1.33)$$

$$= \hbar s \langle \sqrt{N_0} \varphi_0 | \sqrt{N_0} \varphi_0 \rangle \quad (1.34)$$

$$= N_0 \hbar s \quad (1.35)$$

The angular momentum is quantised and proportional to the number of bosons in the BEC fraction/superfluid. We can calculate the velocity field

$$\mathbf{v}_s = \frac{\hbar}{m} \nabla S = \frac{\hbar}{m} \frac{s}{r} \hat{\varphi} \quad (1.36)$$

The streamlines of \mathbf{v}_s are concentric circles, centred around the z -axis, lying in the xy -plane (see Figure 1.4). Contrary to rigid rotation fields which increase proportional to the distance from the z -axis r , the superfluid rotation field decreases proportional to distance from the z -axis $1/r$ and is singular in the origin. Calculating the circulation of the velocity field \mathbf{v}_s along a closed contour including the z -axis gives

$$\oint_{\partial\Sigma} \mathbf{v}_s \cdot d\mathbf{l} = \int_0^{2\pi} \frac{\hbar}{m} \frac{s}{r} \hat{\varphi} \cdot r d\varphi \hat{\varphi} \quad (1.37)$$

$$= 2\pi s \frac{\hbar}{m} \quad (1.38)$$

There are two things to note here. Firstly, the circulation around a closed loop that encompasses the z -axis is quantised in units of \hbar/m for $s \in \mathbb{N}_{>0}$. Secondly, the value of the circulation of the velocity field does not depend on the chosen contour as long as it includes the location of the vortex. This means that all the vorticity is contained at the location where the velocity field is singular (the “core” of the vortex), at $r = 0$ along the z -axis.

Because of the pole in the velocity field, Stokes theorem will lead to the following contradiction

$$2\pi s \frac{\hbar}{m} = \oint_{\partial\Sigma} \mathbf{v}_s \cdot d\mathbf{l} = \iint_{\Sigma} \nabla \times \mathbf{v}_s \cdot d\Sigma = 0 \quad (1.39)$$

and can therefore not be applied. To emphasise that all the vorticity is concentrated around the vortex core one can write formally

$$\nabla \times \mathbf{v}_s = 2\pi s \frac{\hbar}{m} \delta^{(2)}(\mathbf{r}_\perp) \hat{\mathbf{z}}, \quad (1.40)$$

where $\delta^{(2)}$ is 2-dimensional Dirac-delta function and \mathbf{r}_\perp a vector in a plane perpendicular to the vortex line.

1.3 Helium droplets

UNTIL the 1980, most experimental and theoretical work was done on bulk systems, i.e. systems of the order of N_A number of atoms. It was only in the last couple of decades that advancements in technology enabled experimentalists to create nanoscale sized superfluid helium droplets. From the early 1990's onwards, superfluid helium nano-droplets became an active field of study, both experimentally and theoretically.

Finite size effects Helium nanodroplets are considered ideal model systems to explore quantum hydrodynamics in self-contained, isolated superfluids. The main focus has been on the evolution of their properties with the number of atoms in the cluster, until the condensed matter limit is reached. Helium clusters are especially interesting in that quantum effects play a key role in determining their properties. In particular, given that a helium cluster is an ensemble of bosons at about 0.4 K [1, 2], manifestations of collective behaviour (such as superfluidity) are expected. On the other hand, it is not yet clear how the finite size of a cluster affects this non-classical (or degenerate) collective behaviour.

Non-classical ideas to explain, for example the capture of Cs atoms by large helium clusters, were introduced as early as 1986 [3], while recently, Toennies et al. [4] have measured the electronic spectrum of glyoxal molecules embedded in He clusters and found it consistent with a theoretical simulation computed using the phonon dispersion curve of superfluid bulk He II. The authors themselves, however, point out that at the average cluster size of 5500 He atoms reported in [4], the phonon dispersion curve is well in the bulk limit (see also [5, 6]); it is therefore not surprising that they find results consistent with the bulk case, especially for a molecule readily solvated inside the cluster, for which surface effects play a minor role. Therefore the influence on superfluidity of the He clusters size has not been detected so far.

Properties of He droplets are difficult to determine The helium-helium interaction is already weak in bulk liquid helium and in finite self-bound systems such as droplets it is even weaker, e.g. the binding energy per atom is $< 7.17\text{K}$. Because of this helium droplets cool down very rapidly due to fast evaporation and therefore reaching their limiting temperature of about 0.38 K in microseconds. Pure helium droplets are neutral systems and their properties like their size, binding energy and excitation spectra, are not easy to determine experimentally and are usually obtained by indirect methods. This didn't stop the theoreticians describe doped ${}^4\text{He}_N$ droplets using a wide variety of approaches depending on the size and character of the droplets ranging from Quantum Monte Carlo, Hypernetted-Chain/Euler-Lagrange, Variational Monte Carlo and many others.

He droplets will pickup any dopant A key property of helium droplets, in contrast to bulk helium, is their ability to pickup any kind of dopants with which they collide. Depending on the strength of the dopant- ${}^4\text{He}$ interaction and the surface tension of the droplet, a dimensionless parameter λ can be defined^[29] with a critical value $\lambda_0 \sim 1.9$. Below λ_0 impurities are bound to the surface of the droplet (e.g. the alkalies), and above get solvated into the droplet's interior. They can therefore be doped with almost any kind of atomic- or molecular species where they can form new complexes.

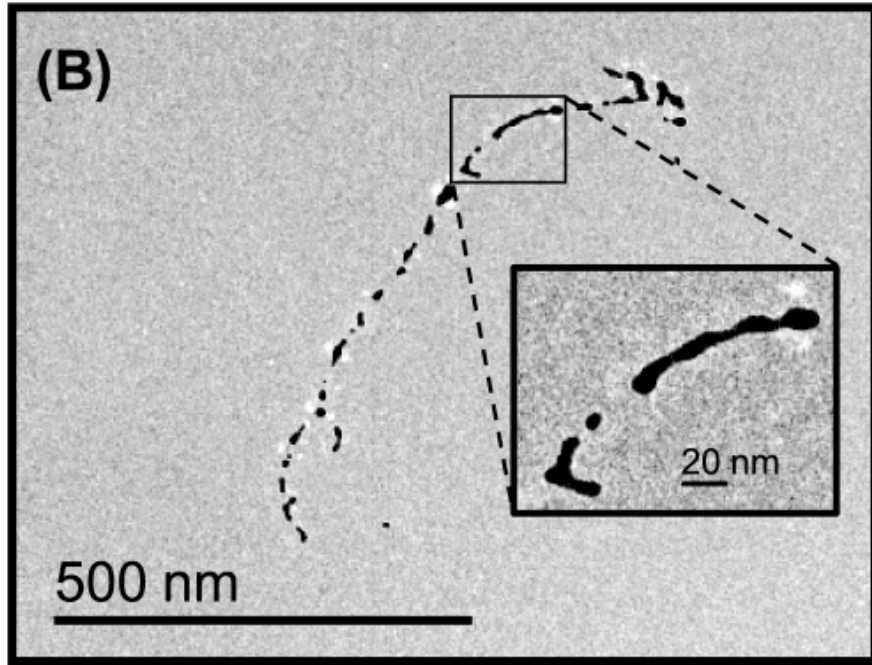


Figure 1.5: Electron-microscope image of an elongated track-shaped Ag-cluster after it is surface-deposited.

This enables a broad spectrum of possible experimental study. Due to the fact that helium droplets are ultra cold superfluid liquids, and therefore provide high mobility of any picked-up dopants, one can do high resolution spectroscopy studies. Having a fine control over the number of picked-up dopants[29] one can use droplets as a matrix for creating self-organising structures of polar molecules, or very cold metal clusters and study their Coulomb explosion.

From the perspective of the droplet it's possible to use the dopants as gentle probes to determine the superfluid properties of helium droplets that would be inaccessible with other methods. For two examples of this see [37-39], where a dopant is used to probe the superfluid character of small ^4He droplets and [16,17] to see their limiting temperatures.

Quantised vortices in He droplets One of the most intriguing properties of superfluid helium droplets is the fact that they can host quantised vortices. Because of their ultra low temperature they are true quantum liquids and their vorticity and angular momentum are quantised. The existence of quantised vortices was anticipated because they have been created and observed in BECs made of dilute gases. However, the detection of quantised vortices is still experimentally challenging.

The last few decades A lot of work has been done on helium droplets the last few decades, both experimentally and theoretically. From the absorption spectra of alkali metal doped helium droplets, the study of doped mixed ^3He - ^4He droplets, electrons in liquid helium, to the investigation of the critical Landau velocity inside small ^4He droplet. For a comprehensive overview of work done in the last two decades, the interested reader is referred to the review papers[JLTP.Vol142.Nos.1/2(2006), IRPC.Vol36No4.621-707(2017), IRPC.Vol33No3.301-339(2014)].

Part I

Photo-excitation dynamics of alkalis

Chapter 2

Alkali-doped nanodroplets

In their 1996 paper^[30] Griffin and Stringari have argued that almost 100% Bose-Einstein Condensation could be achieved in the low density surface region of superfluid He at $T = 0$, as opposed to only about 10% in the bulk. It is therefore evident that a minimally perturbing probe capable of investigating the surface of a He cluster is very desirable.

It comes as no surprise then that alkali atoms are a very natural choice for exactly these type of studies. For example, with a solvation parameter of $\lambda = 0.729$ ^[29], Rb will remain bound to the surface of the droplet. Furthermore, they have a simple, well known, absorption spectrum. They introduce only weak perturbations (alkali-helium interaction energies are on the order of 1 cm^{-1} [8]). Moreover, their simple, one-valence electron structure allows for detailed theoretical modelling. Lastly, theoretical calculations [9, 10] and experimental spectra [11-13] of alkali atoms in bulk liquid helium are available for comparison.

Surprisingly, the study of alkali atoms seeded in highly quantum matrices is relevant to the optimisation of the use of solid hydrogen as a rocket propellant^[31].

Given that the alkalis are ideal probes to probe the boundary region of the nanodroplets, the $np^2\text{P} \leftarrow ns^2\text{S}$ transitions of the alkali atoms have attracted much interest from an experimental and theoretical point of view. The spectroscopy of the higher excited states has been thoroughly explored[32-42]. The obtained spectra can be successfully reproduced by a pseudo-diatomic model[9,21], except for the higher excited states, where the model progressively fails due to the limitations imposed by its realm of validity. While the effect of the excited states on the spectra are now fairly well understood, their influence on the following dynamics is largely unexplored.

In this part of the thesis, the results of the real-time dynamics of a single electronically excited rubidium (Rb) atom, residing in the surface dimple of a helium nano-droplet will be presented. The atom will be excited from its ground state $5s^2\Sigma_{1/2}$ to the $5p^2\{\Sigma, \Pi\}$ and $6p^2\{\Sigma, \Pi\}$ manifold. This will be a combined experimental and theoretical study.

2.1 Experimental setup

A beam of large He clusters is produced in a supersonic expansion from a cold nozzle (Fig. 2.1). The weak He-He binding energy of 7.7 cm^{-1} [22] requires high stagnation

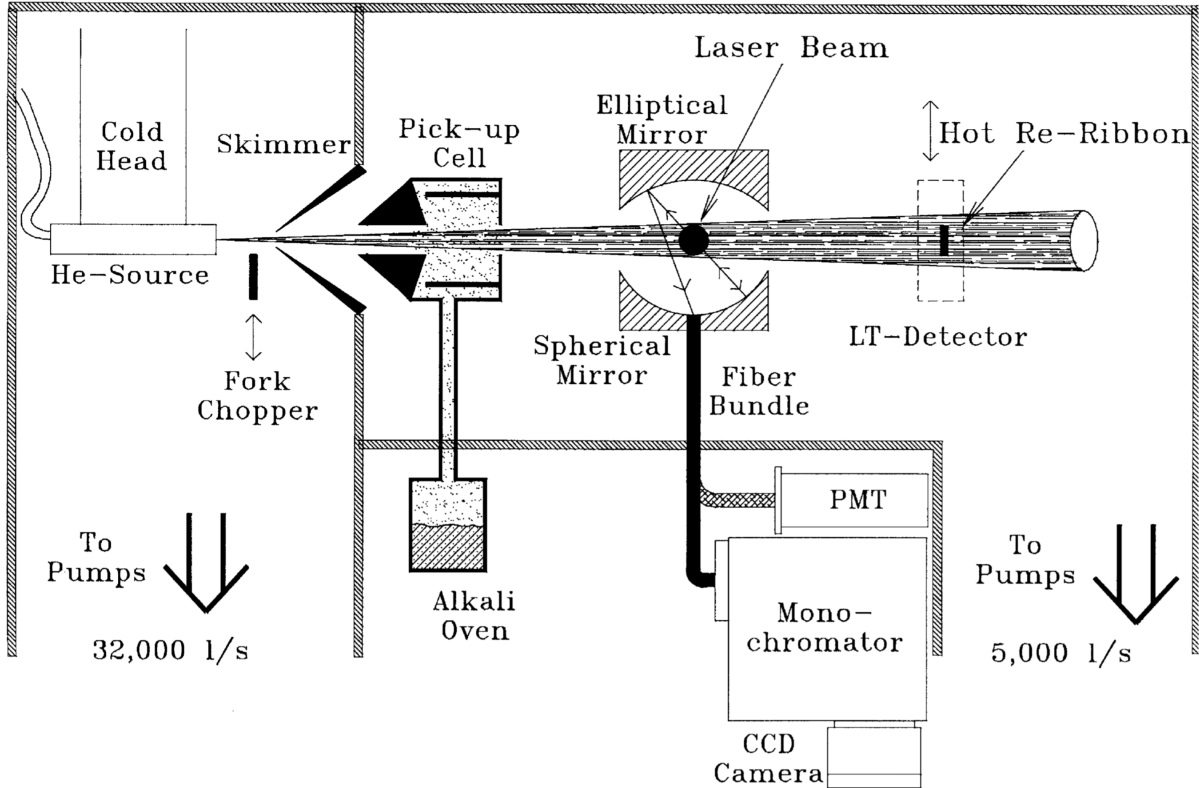


Figure 2.1: Caption

pressures and low nozzle temperatures (T) for large cluster formation. In our apparatus two CTI cryocoolers are used to establish low temperature conditions (down to 12 K) at the source. The first cooler directly cools the nozzle while the second pre-cools the supplied gas. This is needed because, even for small nozzle diameters ($10 \mu\text{m}$), at stagnation pressures up to 10^7 Pa the $1/\sqrt{T}$ dependence of the gas flux leads to heavy gas loads. The pre-cooling system also provides for gas purification. The high gas throughput is easily handled by a 32000 1/s diffusion pump.

At these low temperatures seeding clusters with a chromophore cannot be achieved by co-expansion and the pick-up seeding method becomes necessary [23]. According to this method, the cluster beam is sent through a scattering cell (located a short distance after the skimmer) in which a variable pressure (10^{-3} – 10^{-1} Pa) of the chromophore is maintained by connecting it with an alkali reservoir through a heated tube. The temperature of the pick-up cell, (100 K higher than the reservoir), avoids alkali atom distillation and formation of dimers inside the cell. In their path through the cell the larger clusters pick up alkali atoms without being appreciably deflected. Dissipation of the energy of the captured chromophore is likely to occur by evaporation of He atoms from the clusters, the terminal temperature of which rapidly returns to its pre pick-up value ($\approx 0.4 \text{ K}$) [2].

To probe the picked-up alkali atoms we use laser induced fluorescence (LIF) adopting the photon collection optics design described by Hefter and Bergmann in [24]. The intersection point of the laser and cluster beam from which the fluorescence photons are collected is located a few centimetres downstream of the pick-up cell. The light of the probe laser is introduced in the apparatus via a single mode fibre and focusing optics that makes the laser beam diameter at the crossing point approximately the same as the cluster beam diameter ($\approx 2 \text{ mm}$). To suppress scattered laser light we use a stack of diaphragms forming a baffle of 90 cm length both for the in- and outgoing laser beam. A Woods horn serves as a beam dump. To detect

the fluorescence light originating at the point of intersection, the combination of an elliptical and a spherical mirror is used. These two mirrors focus the emitted photons at the entrance of a fibre bundle. The geometrical collection efficiency is 85% of the 4π solid angle centred around the intersection point. After passing through the fibre bundle, the photons reach a photo-multiplier (PMT) for signal detection. The output pulses of the PMT are (after standard amplification and discrimination) stored using two gated counters which follow the cluster beam chopping frequency. Alternatively, a monochromator (GCA / McPherson, EU-700) coupled to a liquid nitrogen cooled CCD detector (Princeton Instruments, LN/CCD 1152 UV) is used for dispersed fluorescence measurements. The absolute frequency of the probe laser is monitored continuously by a home built wave meter with 0.001 cm^{-1} precision. The amount and angular distribution of alkali atoms carried by the clusters can be monitored by means of a Langmuir-Taylor (LT) surface ionisation detector which is located further downstream and is movable perpendicularly to the cluster beam direction. Since excitation at certain frequencies leads with a significant probability to a desorption of the chromophores from the cluster, we are also able to detect beam depletion spectra. Finally the LT detector provides information on the alkali atom density inside the pick-up cell by measuring the alkali background inside the detection chamber. A computer controls the laser frequency and records the acquisition of photon counts, the actual laser frequency and the parameters for cluster beam and alkali source condition characterisation.

Part II

Capture by quantised vortices

Chapter 3

Quantised vortices in droplets

One of the most unambiguous signatures of the quantum mechanical nature of a substance—and indeed superfluidity—is the appearance of quantised vortices. In contrast to a normal fluid, which will rotate as a solid body when its container moves at low angular velocity, a superfluid will remain at rest. However, above a certain critical angular velocity the thermodynamically stable state of a superfluid includes one or more quantum vortices. Such a vortex can be characterised by a macroscopic wave function and quantised velocity circulation in units of $\kappa = \frac{h}{m}$, where h is Planck's constant and m is the mass of the ^4He atom [2,3]. Recently, the study of vorticity was extended to finite systems such as BECs confined to traps [3,4]. The transfer of energy and angular momentum in finite systems between quantised vortices and surface excitations is of particular interest, as it defines the nucleation dynamics, shape, and stability of the involved vortices [3,4]. In comparison to confined BECs, ^4He droplets are self-contained and present a case for the strongly interacting superfluid. Moreover, the diameter of a vortex core which is approximately 0.2 nm in superfluid ^4He [2] is small relative to the droplet size, suggesting a three-dimensionality of the vortices in droplets. Vorticity in ^4He droplets has therefore attracted considerable interest [5–8].

A schematic of the experiment is shown in Fig. 3.1. Helium droplets are produced by expansion of He, at 20 bar and a temperature $T_0=5.4\text{--}7\text{ K}$, into vacuum through a nozzle of diameter D 1/4 5 "m. The droplets cool rapidly via evaporation and reach a temperature of 0.37 K [20], which is well below the superfluid transition temperature T! 1/4 2:17 K [2,3]. Further downstream, the droplets capture 103–106 Ag atoms in an oven [21]. The droplets are then collided against a thin carbon film substrate at room temperature [21]. Upon impact, the droplets evaporate, leaving on the surface the Ag traces, which are subsequently imaged via a transmission electron microscope (TEM).

Recently, Gomez, Loginov and Vilesov performed experiments[PRL 108, 155302 (2012)] where vortices inside superfluid ^4He droplets, produced by the expansion of liquid helium, were traced by introducing Ag atoms which clustered along the vortex lines, into the droplets. The Ag clusters were subsequently surface-deposited and imaged via electron microscopy. The prevalence of elongated track-shaped deposits (see Figure 1.5) shows that vortices are present in droplets larger than about 300 nm and that their lifetime exceeds a few milliseconds. Two years later Gomez reported[Science 345, 906 (2014)] on the formation of quantum vortex lattices inside droplets. He used single-shot femtosecond x-ray coherent diffractive imaging to investigate the rotation of single, isolated superfluid helium-4 droplets containing $\sim 10^8$ to 10^{11} atoms. The formation of quantum vortex lattices inside the droplets was confirmed by observing the characteristic Bragg patterns from xenon clusters trapped in the vortex cores (see

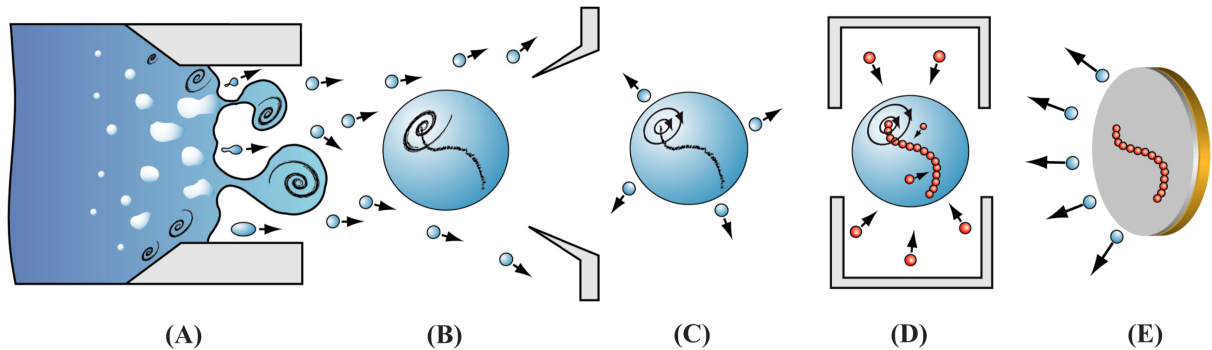


Figure 3.1: Schematic of the experiment. (a) He fluid expands in vacuum and (b) breaks up into rotating droplets. (c) A quantum vortex is formed as a consequence of fast evaporative cooling of the droplet to below T_λ . (d) The droplet is doped with Ag atoms, which are attracted to the vortex core. (e) The droplet then collides with the carbon surface leaving behind the Ag trace, whereas the He evaporates.

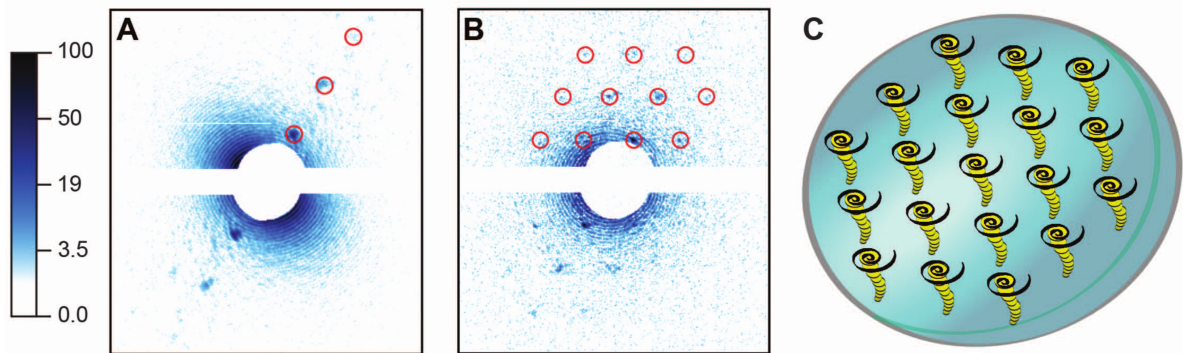


Figure 3.2: He droplets doped with Xe atoms. (A and B) X-ray diffraction images of doped droplets, displayed in a logarithmic intensity scale. (C) Droplet and embedded Xe clusters. Images in (A) and (B) correspond to tilted and parallel alignments of the vortex axes with respect to the incident x-ray beam, respectively.

Figure 3.2).

Bibliography

- [1] P. Kapitza, Nature **141**, 74 (1938), URL <http://dx.doi.org/10.1038/141074a0>.
- [2] B. Rollin and F. Simon, Physica **6**, 219 (1939), ISSN 0031-8914, URL <http://www.sciencedirect.com/science/article/pii/S0031891439800131>.
- [3] W. Keesom and M. A. Keesom, Physica **3**, 359 (1936), ISSN 0031-8914, URL <http://www.sciencedirect.com/science/article/pii/S0031891436803127>.
- [4] L. Tisza, Comptes rendus hebdomadaires des séances de l'Académie des sciences **207**, 1035 (1938), URL <http://gallica.bnf.fr/ark:/12148/bpt6k31590/f1035.item>.
- [5] L. Tisza, Comptes rendus hebdomadaires des séances de l'Académie des sciences **207**, 1186 (1938), URL <http://gallica.bnf.fr/ark:/12148/bpt6k31590/f1186.item>.
- [6] L. Tisza, J. Phys. Radium **1**, 164 (1940), URL <https://doi.org/10.1051/jphysrad:0194000105016400>.
- [7] L. Tisza, J. Phys. Radium **1**, 350 (1940), URL <https://doi.org/10.1051/jphysrad:0194000108035000>.
- [8] P. Lebrun, Cryogenics **34**, 1 (1994), ISSN 0011-2275, fifteenth International Cryogenic Engineering Conference, URL <http://www.sciencedirect.com/science/article/pii/S0011227505800037>.
- [9] W. Keesom and M. A. Keesom, KNAW, Proceedings **35**, 736 (1932), URL <http://www.dwc.knaw.nl/DL/publications/PU00016277.pdf>.
- [10] R. J. Donnelly, Physics Today **62**, 34 (2009), <https://doi.org/10.1063/1.3248499>, URL <https://doi.org/10.1063/1.3248499>.
- [11] H. Kamerlingh Onnes, KNAW, Proceedings **10**, 744 (1908), URL <http://www.dwc.knaw.nl/toegangen/digital-library-knaw/?pagetype=publDetail&pId=PU00013699>.
- [12] H. Kamerlingh Onnes, KNAW, Proceedings **11**, 168 (1909), URL <http://www.dwc.knaw.nl/toegangen/digital-library-knaw/?pagetype=publDetail&pId=PU00013525>.
- [13] P. J. McLennan, H. Smith, and J. Wilhelm, The London, Edinburgh, and Dublin Philosophical Magazine and Journal of Science **14**, 161 (1932), <https://doi.org/10.1080/14786443209462044>, URL <https://doi.org/10.1080/14786443209462044>.
- [14] E. F. Burton, Nature **135**, 265 (1935), URL <http://dx.doi.org/10.1038/135265a0>.
- [15] M. v. Laue, F. London, and H. London, Zeitschrift für Physik **96**, 359 (1935), ISSN 0044-3328, URL <https://doi.org/10.1007/BF01343868>.
- [16] F. Simon, Nature **133**, 529 (1934), URL <http://dx.doi.org/10.1038/133529a0>.

- [17] F. London, Proceedings of the Royal Society of London A: Mathematical, Physical and Engineering Sciences **153**, 576 (1936), ISSN 0080-4630, <http://rspa.royalsocietypublishing.org/content/153/880/576.full.pdf>, URL <http://rspa.royalsocietypublishing.org/content/153/880/576>.
- [18] J. F. Allen, R. Peierls, and M. Zaki Uddin, Nature **140**, 62 (1937), URL <http://dx.doi.org/10.1038/140062a0>.
- [19] J. F. Allen and A. D. Misener, Nature **141**, 75 (1938), URL <http://dx.doi.org/10.1038/141075a0>.
- [20] F. London, Nature **141**, 643 (1938), URL <http://dx.doi.org/10.1038/141643a0>.
- [21] L. Tisza, Nature **141**, 913 (1938), URL <http://dx.doi.org/10.1038/141913a0>.
- [22] L. Landau, Phys. Rev. **60**, 356 (1941), URL <https://link.aps.org/doi/10.1103/PhysRev.60.356>.
- [23] L. Landau, Phys. Rev. **75**, 884 (1949), URL <https://link.aps.org/doi/10.1103/PhysRev.75.884>.
- [24] N. N. Bogolyubov, J. Phys. (USSR) **11**, 23 (1947), [Izv. Akad. Nauk Ser. Fiz. 11, 77 (1947)], URL <https://ufn.ru/ru/articles/1967/11/o/>.
- [25] E. A. Cornell and C. E. Wieman, Rev. Mod. Phys. **74**, 875 (2002), URL <https://link.aps.org/doi/10.1103/RevModPhys.74.875>.
- [26] W. Ketterle, Rev. Mod. Phys. **74**, 1131 (2002), URL <https://link.aps.org/doi/10.1103/RevModPhys.74.1131>.
- [27] D. Mateo, M. Barranco, and J. Navarro, Phys. Rev. B **82**, 134529 (2010).
- [28] R. J. Donnelly, J. A. Donnelly, and R. N. Hills, J. Low Temp. Phys. **44**, 471 (1981).
- [29] F. Ancilotto, P. B. Lerner, and M. W. Cole, J. Low Temp. Phys. **101**, 1123 (1995).
- [30] A. Griffin and S. Stringari, Phys. Rev. Lett. **76**, 259 (1996), URL <https://link.aps.org/doi/10.1103/PhysRevLett.76.259>.
- [31] P. Carrick, ed., *Theoretical Performance of Atomic and Molecular HEDM Additives to Solid H₂*, p. 412 (Proceedings of the High Energy Density Matter (HEDM) Contractor's Conference, Woods Hole, MA.; Edwards Air Force Base, CA, 1993), URL <http://www.dtic.mil/docs/citations/ADA274452>.